ISSN 2316-9281

Scientific Electronic Archives
Issue ID: Vol.19 (3), May/Jun 2026, p. 1-12
DOI: http://dx.doi.org/10.36560/19320262221
+ Corresponding author*:* eric@ufsj.edu.br

Asymptotic connections between Elovich, PFO and PSO adsorption kinetics in a coverage-dependent rate model

Eric Marsalha Garcia, Hosane Aparecida Tarôco, Júlio Onésio Ferreira Melo

Federal University of São João del-Rei

Abstract. The Elovich, pseudo-first-order (PFO), and pseudo-second-order (PSO) equations are widely used in adsorption kinetics, although the connection among them is often treated empirically. Here, we analyze a generalized adsorption rate equation in which the apparent adsorption coefficient decreases exponentially with surface coverage. The model recovers Elovich behavior at low coverage and yields effectively PFO- or PSO-like relaxation near equilibrium, depending on the magnitude of a composite coverage parameter. It also predicts an intermediate regime in which neither pseudo-order approximation is fully adequate. Application to representative literature datasets shows that this approach provides a practical tool for interpreting why different empirical fits succeed in different coverage domains and why some kinetic curves require direct numerical treatment. The framework is therefore best viewed as an effective tool for kinetic interpretation and regime classification rather than as a microscopic theory of surface heterogeneity.
Keywords: Adsorption kinetics; coverage-dependent rate coefficient; Elovich equation; pseudo-order kinetics; batch adsorption; kinetic modeling

Introduction

Over more than a century, kinetic models have been employed to understand the time evolution of adsorption processes and the conditions under which equilibrium is attained (Lagergren, 1898; Azizian, 2004; Marczewski, 2010; Zhang, 2023; Salvestrini, 2018; Huang and Shih, 2025). In this context, a key quantity is the adsorbed amount per unit mass of adsorbent, $q(t)$, whose time dependence reflects the progressive occupation of adsorption sites until equilibrium is approached. For batch adsorption systems, this behavior can be described in parallel through the fractional surface coverage, $\theta(t)$, and through the variation of the solute concentration in the liquid phase, $C(t)$, which evolves from the initial concentration, C_0, to the equilibrium concentration, C_e.

$$\theta(t) = \frac{q(t)}{q_{\max}} \ (Eq. 1)$$

A common mechanistic starting point is the elementary Langmuir adsorption step (Eq. 2), which, when expressed in differential form in terms of fractional surface coverage, leads to the classical Langmuir kinetic equation (Eq. 3). In this formulation, $k_a$denotes the adsorption rate coefficient, which governs the frequency with which solute molecules collide with and occupy vacant sites, whereas $k_d$represents the desorption rate coefficient associated with the reverse process, in which an occupied site releases its adsorbed species back into solution. Here, Adenotes the solute in solution, Sa vacant adsorption site, and ASan occupied site.

$$A + S \rightleftharpoons AS \ (Eq. 2)$$
$$\frac{d\theta}{dt} = k_a C(t)(1-\theta) - k_d\theta \ (Eq. 3)$$

In many batch adsorption systems, adsorption is accompanied by measurable solute depletion in the liquid phase. Under these conditions, the concentration in solution may be related to the fractional surface coverage through the linear mass-balance expression given in Eq. 4, where $\beta_A$represents the decrease in solute concentration per unit increase in fractional

coverage. This parameter may be written either in terms of the equilibrium concentration change (Eq. 5) or in terms of the monolayer adsorption capacity, adsorbent dosage, and solution volume (Eq. 6).

$$C(t) = C_0 - \beta_A \theta(t) \quad (\text{Eq. } 4)$$

$$\beta_A = \frac{C_0 - C_e}{\theta_e} (\text{Eq. } 5)$$

$$\beta_A = \frac{q_{\max} m_s}{V} (\text{Eq. } 6)$$

Within this classical framework, two simplified kinetic equations have become widely used in the adsorption literature: the pseudo-first-order (PFO) model (Eq. 7) and the pseudo-second-order (PSO) model (Eq. 8). The PFO equation, originally introduced by Lagergren (1898), assumes that the adsorption rate is proportional to the deviation from equilibrium, leading to an exponential approach toward q_e. The PSO equation, in contrast, assumes a quadratic dependence on the same driving force, resulting in the familiar hyperbolic approach to equilibrium (Azizian, 2004; Azizian and Yahyaei, 2006; Azizian and Bashiri, 2008; Ghaedi et al., 2014; Marczewski, 2010; Marczewski et al., 2018; Marczewski et al., 2013; Zhang, 2023; Al-Ghouti and Da'ana, 2020; Salvestrini, 2018; Huang and Shih, 2025).

$$\frac{dq}{dt} = k_1(q_e - q) \qquad \text{(Eq. 7)}$$

$$\frac{dq}{dt} = k_2(q_e - q)^2 \qquad \text{(Eq. 8)}$$

Although PFO and PSO equations are often treated as empirical curve-fitting models, both can be derived as limiting forms of the full Langmuir kinetic equation (Eq. 3) under specific conditions. Azizian (2004) demonstrated that inclusion of the solute depletion term (Eq. 4) leads to a quadratic relaxation law capable of producing PSO-like behavior, whereas neglect of depletion yields an effective first-order expression. Marczewski (2010) later showed that the corresponding Langmuir-type rate equation admits a complete analytical solution, with subsequent extensions to adsorption and desorption systems reported in later studies (Marczewski et al., 2013; Marczewski et al., 2018).

Building on these developments, Zhang (2023) proposed a particularly useful set of dimensionless criteria to determine when the classical pseudo-first-order and pseudo-second-order expressions can approximate the full Langmuir kinetic trajectory. In her analysis, the kinetic classification is reduced to the ratio between the two characteristic roots of the Langmuir quadratic rate equation, θ_{e1}/θ_{e2}, which depends only on the combinations $C_0/\beta_A$and $K_L\beta_A$. When $\theta_{e1}/\theta_{e2} \to 0$, the contribution of the quadratic term becomes negligible and the dynamics reduce to an effective pseudo-first-order law. Here, $K_L$is the Langmuir affinity constant, which reflects the strength of interaction between solute molecules and adsorption sites. According to this framework, the PFO limit can be reached only under the following three scenarios:

a) $C_0/\beta_A \to 0$, corresponding to very low solute supply relative to adsorption capacity;

b) $C_0/\beta_A \to \infty$, corresponding to overwhelming solute excess;

c) $K_L\beta_A \to 0$, which reflects extremely weak binding.

Conversely, PSO-like behavior requires $\theta_{e1}/\theta_{e2} \to 1$, a condition achieved only when $C_0/\beta_A = 1$ and simultaneously $K_L\beta_A \to \infty$. In other words, the classical PSO limit appears only when the solute concentration is perfectly matched to the adsorbent capacity and the binding affinity diverges—conditions that are mathematically pristine but practically unattainable in real systems.

However, these criteria apply only in narrow limiting regimes, such as strong depletion or near-saturation conditions, which may not always be representative of experimentally sampled adsorption trajectories. At the same time, many adsorption studies continue to report PSO as the best-fitting model across a wide variety of systems (Azizian, 2004; Al-Ghouti and Da'ana, 2020; Huang and Shih, 2025; Zohra et al., 2025; Liu et al., 2010; Luo et al., 2015; Khare and Kumar, 2012). This recurring empirical success suggests that second-order-like behavior may appear under broader practical conditions than those predicted by the classical limiting derivations alone.

This observation motivates the present work. Rather than proposing a new microscopic theory of adsorption, we examine a generalized coverage-dependent rate equation in which the apparent adsorption coefficient decreases exponentially with surface coverage. Within this formalism, the low-coverage limit recovers the Elovich equation, the near-equilibrium region may become effectively PFO- or PSO-like depending on the magnitude of a composite coverage parameter, and an intermediate regime naturally emerges in which neither pseudo-order approximation is expected to remain fully adequate. From this perspective, Elovich, PFO, and PSO are better interpreted as limiting kinetic descriptions associated with different regions of the adsorption trajectory rather than as rigidly competing models.

Coverage-dependent activation energy and the Elovich rate coefficient

We assume that the adsorption rate coefficient follows an Arrhenius-type expression whose activation energy increases linearly with the

local adsorbed amount. Accordingly, the coverage-dependent rate constant is written as:

$$k = k_0 e^{-(E_0+\tilde{\beta}q)/(RT)} (\text{Eq. } 9)$$

where $k_0$is the pre-exponential factor, $E_0$is the intrinsic activation energy at zero coverage, and $\tilde{\beta}$ quantifies the growth of the activation barrier with the amount already adsorbed. Introducing the compact notation $\alpha = k_0 e^{-E_0/(RT)}$and redefining the heterogeneity parameter as $\beta = \frac{\tilde{\beta}}{RT}$, Eq. 9 reduces to Eq. 10:

$$k = \alpha e^{-\beta q} \qquad (Eq. 10)$$

This corresponds to an Elovich-type rate coefficient. Here, α controls the intrinsic low-coverage rate, while β quantifies the energetic heterogeneity. A small β describes nearly homogeneous surfaces, whereas a large β produces strong curvature and PSO-like characteristics. This structure parallels the Temkin, Frumkin, and Butler–Volmer models in interfacial electrochemistry, where energetic heterogeneity similarly manifests through coverage-dependent activation barriers.

Embedding Elovich kinetics into the Langmuir adsorption step

The irreversible Langmuir rate expression for fractional coverage follows directly from the forward step of the elementary adsorption mechanism. Neglecting desorption and writing the kinetics in terms of the fractional occupation of surface sites leads to Eq. 11 and, equivalently, for the uptake $q = q_e\theta$, to Eq. 12:

$$\frac{d\theta}{dt} = k\, C(t)(1-\theta) \qquad (Eq. 11)$$

$$\frac{dq}{dt} = k\, C(t)(q_e - q) \qquad (Eq. 12)$$

By substituting the Elovich dependence from Eq. 10, one obtains the generalized Langmuir–Elovich (GLE) kinetic equation:

$$\frac{dq}{dt} = \alpha C(t) e^{-\beta q}(q_e - q) \;\; (Eq. 13)$$

Although the analytical reductions derived from Eq. 13 already represent an important conceptual result, by revealing how classical kinetic laws emerge as limiting cases of a single mechanistic rate equation, their use should ideally be complemented by numerical integration of the full differential equation. In the general case, Eq. 13 does not admit a simple closed-form solution in elementary functions, and numerical integration is required to capture the exact time evolution of $C(t)$ and to fully resolve the coupled effects of coverage, heterogeneity, and solute depletion.

Nevertheless, for preliminary interpretation, it remains instructive to examine the asymptotic limits of Eq. 13. Within this unified framework, the low-coverage limit reproduces an Elovich-type law, the near-equilibrium expansion yields PFO- and PSO-like forms, and the intermediate regime naturally exhibits mixed-order kinetics. Thus, Elovich, PFO, and PSO should not be regarded as independent kinetic models, but rather as limiting manifestations of a more general rate law.

Kinetic regimes emerging from the generalized rate law

The GLE kinetic equation (Eq. 13) naturally generates three mechanistic regimes along the adsorption trajectory: a low-coverage Elovich region, an intermediate mixed-order region, and a high-coverage near-equilibrium domain. Only in this latter domain does the asymptotic structure underlying pseudo-first- and pseudo-second-order kinetics become valid.

To analyze the approach to equilibrium in a unified way, it is convenient to introduce the deviation from equilibrium, $\varepsilon = q_e - q$,which quantifies how far the system remains from its asymptotic state. Small values of εcorrespond to the high-coverage region where pseudo-order behavior emerges, whereas large ε characterize the early Elovich-type stage of the trajectory.

Elovich regime (low coverage; $C \approx C_0$; ε large)

When the uptake remains in the very early stages of adsorption, the system explores a regime where less than thirty percent of the available capacity has been filled. Mathematically, this corresponds to Eq.14:

$$\frac{q(t)}{q_e} < 0.3 \qquad \text{(Eq. 14)}$$

The deviation from equilibrium, $\varepsilon = q_e - q$, remains effectively constant throughout this early stage. In this low-coverage limit, the number of vacant sites is large and solute depletion in the liquid phase is negligible, which justifies the approximation $C(t) \approx C_0$. Under these conditions, the generalized Langmuir–Elovich (GLE) kinetic equation (Eq. 13) simplifies to Eq. 15, which is the standard Elovich form (Eq. 16) with $a = \alpha C_0 q_e$ and $b = \beta$. In this regime, the kinetics are mechanistically Elovich and pseudo-order behavior cannot arise.

$$\frac{dq}{dt} \approx (\alpha C_0 q_e) e^{-\beta q}, \qquad \text{(Eq. 15)}$$

$$\frac{dq}{dt} = a e^{-bq}, \qquad \text{(Eq.16)}$$

This result shows that the Elovich equation is not an empirical assumption, but the natural low-coverage limit of the generalized GLE kinetic equation.

Near-equilibrium expansion (high coverage; $C \approx C_{eq}$; $\varepsilon \ll 1$)

When the trajectory reaches a sufficiently advanced stage, such that the relative uptake

exceeds the threshold defined in Eq. (17), the system enters a regime where the deviation from equilibrium, $\varepsilon = q_e - q$, becomes small and the kinetic trajectory evolves increasingly slowly. In this late-time domain, concentration variations in the liquid phase are negligible, allowing the approximation $C(t) \approx C_{eq}$.

$$\frac{q(t)}{q_e} > 0.7 \qquad \text{(Eq. 17)}$$

To obtain an analytical description of the late-time relaxation, it is convenient to rewrite the GLE kinetic equation (Eq. 13) in terms of a single function that collects all coverage-dependent contributions. This is done by introducing the composite function $f(q)$ in Eq. (18), which allows the rate law to be written compactly as $dq/dt = f(q)$.

$$f(q) = \alpha C(q)(q_e - q)e^{-\beta q} \qquad (Eq. 18)$$

The near-equilibrium behavior is then obtained by performing a Taylor expansion of $f(q)$ around $q = q_e$, as expressed in Eq. (19). Since $f(q_e) = 0$, only the first derivative contributes to the leading term of the expansion, yielding the simplified linear form given in Eq. (20). Because the relaxation time satisfies $\Delta t = \Delta q/f(q)$, the limit $f(q) \to 0$implies $\Delta t \to \infty$, which explains the long late-time tail observed experimentally.

$$f(q) \approx f(q_e) + f'(q_e)(q - q_e), \qquad \text{(Eq. 19)}$$

$$f(q) \approx f'(q_e)(q - q_e), \qquad \text{(Eq. 20)}$$

To make the deviation from equilibrium explicit, we introduce $\varepsilon = q_e - q$ and substitute $q = q_e - \varepsilon$ into the generalized rate law, obtaining Eq. (21). For small ε, the exponential factor can be linearized as in Eq. (22).

$$\frac{dq}{dt} = C_{eq}\,\alpha\, e^{-\beta q_e}\, e^{\beta\varepsilon}\,\varepsilon, \qquad \text{(Eq. 21)}$$

$$e^{\beta\varepsilon} \approx 1 + \beta\varepsilon, \qquad \text{(Eq. 22)}$$

Finally, defining the constant $A = C_{eq}\alpha e^{-\beta q_e}$ in Eq. (23) and substituting back into Eq. (21) leads to the generalized near-equilibrium GNE kinetic equation, written in Eq. (24), which will be used to classify the pseudo-order regimes.

$$A = C_{eq}\alpha e^{-\beta q_e}, \qquad \text{(Eq. 23)}$$

$$\frac{dq}{dt} = A\varepsilon + \beta A\varepsilon^2 \qquad \text{(Eq. 24)}$$

Pseudo-first-order limit

Although the local condition for linearization is $\beta\varepsilon \ll 1$, this criterion is not convenient because $\varepsilon(t)$ varies along the kinetic trajectory. Since $0 \le \varepsilon(t) \le q_e$, a sufficient global condition for the dominance of the linear term is $\beta q_e \ll 1$. Under this condition, $\beta\varepsilon(t)$ remains small for all times, and the generalized near-equilibrium equation reduces consistently to the PFO form. The product βq_e therefore plays a central role and is hereafter referred to as the heterogeneity parameter.

Consequently, the GNE kinetic equation reduces to the linear form given by Eq. 25, whose solution is provided by Eq. 26:

$$\frac{dq}{dt} \approx A(q_e - q), \qquad \text{(Eq. 25)}$$

$$q(t) = q_e(1 - e^{-At}). \qquad \text{(Eq. 26)}$$

Thus, $\beta q_e \ll 1$ offers a practical and experimentally accessible criterion for first-order–dominated kinetics. When the product of the heterogeneity parameter β and the equilibrium capacity q_e is sufficiently small, the energetic landscape becomes effectively homogeneous and the approach to equilibrium acquires a strictly monoexponential character, defining the PFO-dominated regime.

Pseudo-second-order limit

When the global heterogeneity parameter $\beta q_e$is much larger than unity, the nonlinear channel dominates the entire kinetic trajectory. In this regime, the condition $\beta\varepsilon \gg 1$ holds over most of the high-coverage domain, since $0 \le \varepsilon(t) \le q_e$and its minimum value is approached only asymptotically as $\varepsilon \to 0$. As a consequence, the linear pathway becomes dynamically irrelevant and the generalized rate law reduces to the heterogeneous quadratic form given by Eq. 27, whose solution is provided by Eq. 28:

$$\frac{dq}{dt} \approx \beta A(q_e - q)^2 \qquad \text{(Eq. 27)}$$

$$q(t) = \frac{\beta A q_e^2\, t}{1 + \beta A q_e\, t} \qquad \text{(Eq. 28)}$$

This hyperbolic approach is the hallmark of pseudo-second-order–dominated behavior. A system is therefore PSO-dominated when $q/q_e >$ 0.7and $\beta q_e \gg 1$, since under these conditions the heterogeneous activation landscape overwhelms the linear relaxation channel. As a result, the kinetics are governed by a quadratic dependence on the remaining capacity, giving rise to the characteristic PSO-like uptake profile.

Determination of β from ln(k/C_{eq}) analysis

The generalized near-equilibrium (GNE) kinetic equation (Eq. 24) shows that the late-time dynamics are governed by an effective rate coefficient of the form given by Eq. 29, where βquantifies the growth of the activation barrier with surface coverage.

This structure implies that, whenever the solution concentration varies only weakly in the high-coverage region, the dimensionless ratio k_{eff}/C_{eq}decays exponentially with coverage. Taking the logarithm of this exponential dependence leads directly to the linear relation expressed in Eq. 30. In practice, this analysis is therefore restricted to the late-time portion of the kinetic trajectory, after the system has left the mixed-order intermediate regime and entered the near-equilibrium domain where pseudo-order behavior emerges.

$$k_{\mathrm{eff}}(q) = C_{eq}\,\alpha\, e^{-\beta q} \qquad \text{(Eq.29)}$$

$$\ln\left[\frac{k_{\mathrm{eff}}}{C_{eq}}\right] = \ln(\alpha) - \beta\, q_e \qquad (Eq.30)$$

Equation 30 provides a direct experimental route for determining $\beta$from uptake data. In practice, the effective rate constant $k$is obtained by fitting the near-equilibrium tail of the kinetic trajectory to either the pseudo-first-order (PFO) or pseudo-second-order (PSO) expression, using only data points with $q/q_e \gtrsim 0.7$. The distinction lies solely in which relaxation channel dominates: for kinetically homogeneous surfaces ($\beta\varepsilon \ll 1$), the fitted $k$reflects the PFO-like linear channel, whereas for strongly heterogeneous surfaces ($\beta\varepsilon \gg 1$), the fitted $k$reflects the PSO-like quadratic channel.

Regardless of which channel provides the observable k, substitution into Eq. 30 yields the same linear relation, so that a plot of $\ln(k/C_{eq})$versus $q_e$produces a straight line with slope $-\beta$. The intercept retains information on the intrinsic prefactor α, while the slope provides a quantitative measure of the coverage-dependent activation penalty.

This unified $\ln(k/C_{eq})$ analysis demonstrates that the extracted β is independent of whether the late-time kinetics appear PFO- or PSO-like in conventional empirical fits. Both behaviors arise as limiting expressions of the same generalized kinetic law and inherit the exponential attenuation structure encoded in Eq. 29. Importantly, this method is not applicable to the early or intermediate portions of the trajectory, where mixed-order behavior prevails and pseudo-order approximations break down. It must therefore be restricted to data acquired in the high-coverage, near-equilibrium regime.

In this sense, pseudo-order fits do not determine β; rather, βdetermines which pseudo-order form becomes observable once the system enters the near-equilibrium domain. This provides a unifying and quantitative criterion for kinetic regime classification and a robust route for estimating energetic heterogeneity from standard adsorption experiments.

Derivation of βq_e from exact solution of GNE kinetic equation

When the parameter β cannot be obtained from the $\ln(k/C_{eq})$ analysis because only a single kinetic curve is available, the alternative is to extract the composite quantity βq_edirectly from the full analytical solution of the generalized rate law. To obtain this closed-form expression, we start from the coverage-based formulation of the GNE kinetic equation (Eq. 24). This expression contains both the intrinsic first-order contribution $A\varepsilon$ and the coverage-dependent attenuation encoded in the nonlinear term $\beta A\varepsilon^2$. In the sequence below we present the logical steps used to obtain the closed-form analytical solution of Eq. 24.

Step 1 — Transformation to the error variable $\varepsilon(t)$

Using $\varepsilon = q_e - q$, Eq. 24 can be rewritten in the form shown in Eq. 31.

$$\frac{d\varepsilon}{dt} = -\frac{dq}{dt} = -A\varepsilon(1+\beta\varepsilon). \qquad \text{(Eq. 31)}$$

Equation (Eq. 31) is a Riccati-type differential equation, but crucially it is *separable*. This transformation shows that the nonlinear kinetics are governed by a rational function of ε, which can be integrated exactly.

Step 2 — Partial fraction decomposition

The denominator factorizes naturally, yielding the expression in Eq. 32.

$$\frac{1}{\varepsilon(1+\beta\varepsilon)} = \frac{1}{\varepsilon} - \frac{\beta}{1+\beta\varepsilon}. \qquad \text{(Eq. 32)}$$

This decomposition is the key technical step enabling the analytical solution. Integrating both sides gives Eq. 33, where C is the integration constant. Exponentiation then yields the implicit relation given by Eq. 34.

$$\ln|\,\varepsilon\,| - \ln|\,1+\beta\varepsilon\,| = -At + C \qquad \text{(Eq. 33)}$$

$$\frac{\varepsilon}{1+\beta\varepsilon} = Ke^{-At}, K = e^{C}. \qquad \text{(Eq. 34)}$$

Eq. 34 represents the general solution of the kinetic equation obtained prior to applying the boundary conditions.

Step 3 — Solving explicitly for $\varepsilon(t)$

Rearranging Eq. 34 yields the rational form (Eq. 35):

$$\varepsilon(t) = \frac{K\,e^{-At}}{1-\beta K\,e^{-At}}. \qquad \text{(Eq. 35)}$$

This expression already captures the essential physics: the exponential decay is modified by a denominator that depends on β, which slows the approach to equilibrium in heterogeneous systems.

Step 4 — Applying the boundary condition $q(0) = 0$

For batch adsorption starting from a clean surface, the initial condition is: $q(0) = 0 \Rightarrow \varepsilon_0 = q_e$. Evaluating Eq. 35 at $t = 0$ directly yields the value of K(Eq. 36).

$$q_e = \frac{K}{1 - \beta K} \Rightarrow K = \frac{q_e}{1 + \beta q_e}. \qquad \text{(Eq. 36)}$$

This step removes the integration constant entirely and makes the solution depend only on the physical parameters A, β, and q_e. Substituting Eq. 36 back into Eq. 35 yields Eq. 37.

$$\varepsilon(t) = \frac{q_e e^{-At}}{1 + \beta q_e \,[1 - e^{-At}]}. \qquad \text{(Eq. 37)}$$

Step 5 — Introducing the composite parameter $B = \beta q_e$

Because the kinetic solution contains β only through the combination βq_e, it is natural to define:

$$B = \beta q_e. \qquad \text{(Eq. 38)}$$

With this substitution, Eq. 37 becomes:

$$\varepsilon(t) = \frac{q_e e^{-At}}{1 + B(1 - e^{-At})}. \qquad \text{(Eq. 39)}$$

This expression makes it explicit that $\beta$and $q_e$never appear independently in the exact solution of the generalized rate law. The parameter constrained by kinetic data is therefore not β alone, but the composite quantity $B = \beta q_e$. This is the mathematical origin of the identifiability limitation discussed in the main text: different pairs (β, q_e) that share the same value of B produce indistinguishable kinetic traces, making only the product βq_ean observable kinetic parameter.

Step 6 — Final reduced analytical solution

Because $q(t) = q_e - \varepsilon(t)$, we obtain the compact closed form (Eq. 40):

$$\boxed{q(t) = q_e - \frac{q_e e^{-At}}{1 + B(1 - e^{-At})}} \qquad \text{(Eq. 40)}$$

This is the reduced analytical solution used in the fitting procedure. It depends only on the physically meaning full parameters:

- ✓ A: intrinsic rate constant,
- ✓ q_e: independently measured equilibrium uptake,
- ✓ $B = \beta q_e$: the composite heterogeneity parameter directly identifiable from kinetic data.

Thus, the integrated form offers a transparent and mathematically rigorous route to quantify energetic heterogeneity directly from experimental trajectories, while circumventing the structural non-identifiability inherent to empirical pseudo-order formulations. It should be emphasized, however, that this closed-form expression is strictly applicable in the near-equilibrium domain. Outside this regime, the GLE kinetic equation in Eq. 13 must be integrated numerically.

Thus, the integrated form provides a transparent and mathematically rigorous route to quantify energetic heterogeneity directly from experimental trajectories, while circumventing the structural non-identifiability inherent to empirical pseudo-order formulations. It should be emphasized, however, that this closed-form expression is strictly valid only in the near-equilibrium domain. Outside this regime, the GLE kinetic equation given by Eq. 13 must be treated by numerical integration.

To place these results in context, Figure 1 presents a unified schematic of the generalized Langmuir–Elovich kinetics, illustrating how the fundamental rate law branches into low-coverage, intermediate, and near-equilibrium regimes. The diagram shows how the classical Elovich, PFO, and PSO expressions emerge as limiting cases of a single governing equation, while highlighting the distinct parameter-identification strategies associated with datasets acquired at a single initial concentration (numerical integration) and at multiple initial concentrations (linear extraction of β from $\ln(k_{\mathrm{eff}}/C_{eq})$).

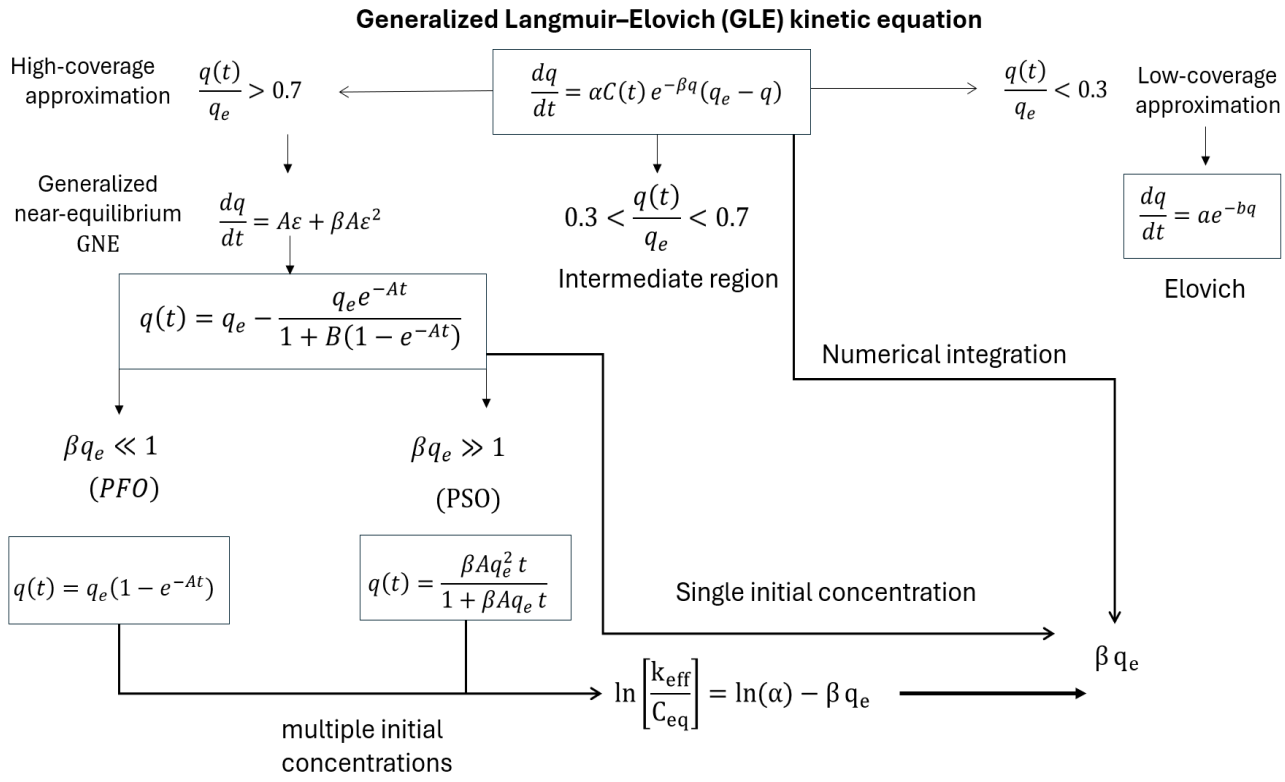

Figure 1- Summary of the kinetic regimes generated by the generalized Langmuir–Elovich rate law. The scheme shows how low-coverage, mixed-order, and near-equilibrium limits emerge from the same governing equation, recovering exponential, PFO, and PSO behaviors as natural asymptotic cases.

Contextualization and analysis

The following case studies present representative adsorption kinetic datasets extracted from the published literature. All experimental data points were digitized directly from the original figures using WinPlotDigitizer prior to analysis. The study by Zohra et al., (2025) was selected to illustrate the application of the $\ln(k_{\text{eff}}/C_{eq})$approach, as the authors reported kinetic measurements performed at multiple initial concentrations. References 14–16 correspond to studies previously cited by Zhang (Zhang, 2023) and were included here to enable a direct comparison between the conclusions drawn from Zhang's classification scheme and those obtained using the present generalized framework

Zohra et al. (2025)

To establish a concrete reference point for applying the GLE kinetic equation framework, we selected a representative literature dataset reporting the adsorption kinetics of Congo Red onto a low-cost lignocellulosic biosorbent. In the study of Zohra et al., (2025), the authors investigated the uptake of Congo Red at initial concentrations ranging from 150 to 300 mg L^{-1}, using a fixed sorbent dosage of 1 g L^{-1} and monitoring the contact time for up to 120 minutes. This dataset was specifically selected because the authors performed adsorption experiments at different initial dye concentrations, providing a robust basis for testing how the kineticparameters evolve with solute loading. Moreover, the experimental conditions are well controlled and the resulting kinetic curves exhibit the characteristic transition from rapid early uptake to a slow approach to equilibrium.

To analyze the coverage domain sampled by the experiment, digitized kinetic data for the 300 mg L^{-1} system were extracted using PlotDigitizer. Figure 2 shows the resulting normalized uptake $q(t)/q_e$ as a function of time. The dashed horizontal line marks the threshold $q(t)/q_e = 0.7$, which approximately separates the intermediate-coverage domain from the high-coverage asymptotic regime in the Generalized Langmuir–Elovich model. A simple residence-time analysis reveals that approximately 97% of the total experimental duration occurs with $q(t)/q_e > 0.7$. Under these conditions, the trajectory crosses the intermediate Elovich-like region almost instantaneously and evolves almost entirely within the high-coverage domain.

Consequently, an Elovich-dominated relaxation is incompatible with the coverage range actually sampled by the experiment. Instead, the kinetics must be governed by one of the pseudo-first-order or pseudo-second-order asymptotes of the generalized model, rather than by a genuine Elovich law.

To construct the $\ln(k/C_{eq})$ plots shown in Figure 3, the equilibrium solution concentrations C_{eq} were first reconstructed from the adsorption mass balance. Using these reconstructed values, the logarithmic ratios $\ln(k_1/C_{eq})$ and $\ln(k_2/C_{eq})$ were evaluated for all initial dye concentrations reported in the original publication.

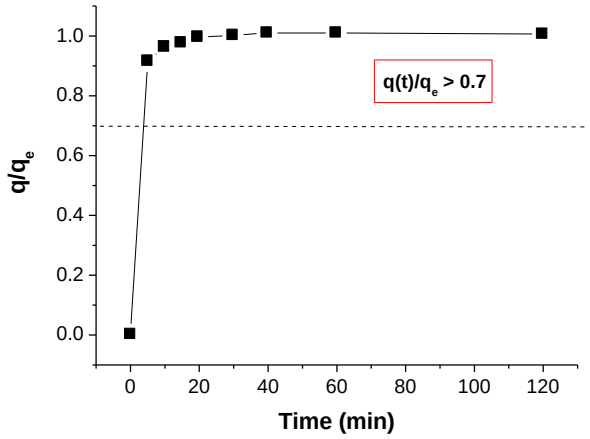

Figure 2. Normalized uptake $q(t)/q_e$ for the 300 mg L⁻¹ kinetic experiment. Data points (■) were extracted from the original publication (Zohra et al., 2025) using PlotDigitizer. The dashed line marks the threshold $q(t)/q_e = 0.7$, and approximately 97% of the experimental time window lies above this value, indicating that the trajectory remains almost entirely within the high-coverage regime.

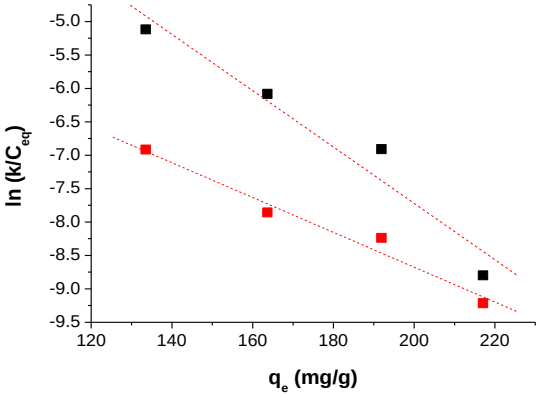

Figure 3. Linear $\ln(k/C_{eq})$ vs. q_e relationships obtained from the pseudo-first-order (■) and pseudo-second-order kinetic (■) constants reported by Zohra *et al.* (2025). Both regressions give consistent β values (Eq. 30), indicating that the system lies in the high-coverage, PSO-dominated regime.

To further contextualize the kinetic regime of the system studied by Zohra et al.,(2025), we also evaluated the classical classification parameter proposed by Zhang (Zhang, 2023). In this framework, the kinetic regime is determined by the dimensionless solute-to-capacity ratio $C_0/\beta_A = \frac{C_0}{q_{\max} m_s/V}$. Using the experimental conditions reported in the original article, the value of C_0/β_A spans the interval 0.39–1.16 across the four concentrations investigated. According to Zhang's classification criterion (Zhang, 2023):

- ✓ $C_0/\beta_A \to 0$ or $C_0/\beta_A \to \infty$corresponds to PFO-dominated kinetics, whereas
- ✓ Values close to unity, i.e., $C_0/\beta_A \approx 1$, are expected to produce PSO-like behavior.

Within this framework, PSO dominance would be predicted only for the 300 mg·L⁻¹ system, as it is the sole condition where the ratio C_0/β_A approaches unity. Notably, this is indeed the concentration for which Zohra et al., (2025) reported the best pseudo-second-order fit, exhibiting a higher R^2 relative to the PFO model.

In contrast, applying our criterion based on the product βq_e, obtained from the $\ln(k/C_{eq})$ analysis, indicates that the values for this system lie in the range 3.5–9.1, considering the β estimates derived from both $k_1$and k_2. Although these values are not exceedingly large, they are sufficiently greater than unity to place the system beyond the PFO domain. Accordingly, within the Generalized Langmuir–Elovich framework, the expected kinetic behavior would be closer to pseudo-second-order across all concentrations investigated, rather than only at the highest concentration.

Interestingly, this prediction aligns exactly with the experimental behavior reported in the original study: for every concentration examined (150–300 mg L⁻¹), the authors obtained pseudo-second-order fits with $R^2 \approx 0.999$, whereas the pseudo-first-order model systematically performed worse.

Thus, while Zhang's criterion would classify only a single concentration as PSO-dominated, our model correctly identifies all kinetic traces as belonging to the high-coverage, quadratic regime. Moreover, it is worth emphasizing that Zhang's framework does not provide any prediction regarding the surface-coverage factor and therefore cannot discriminate between competing heterogeneous formulations (e.g., Elovich-type alternatives), a capability that is naturally embedded in the Generalized Langmuir–Elovich model.

Liu et al.,(2010)

In the study of Liu et al.,(2010), phenol adsorption onto activated carbon fibers was investigated under a single set of experimental conditions, without kinetic measurements at multiple initial concentrations. This dataset was deliberately selected because it represents the opposite scenario to that of Zohra et al., (2025). Because Liu et al., (2010) did not perform kinetic measurements at multiple initial concentrations, the concentration-dependent procedure required to extract $-\beta$ from Eq. (30) cannot be applied.

In this situation, the near-equilibrium exact solution (Eq. 40) must therefore be applied to obtain β. Figure 4 shows the kinetic points extracted using WinPlotDigitizer from the original work of Liu et al., (2010), together with the fit obtained from the exact integrated form. Notably, the vast majority of the kinetic trace lies in the region $q(t)/q_e > 0.7$, indicating that the system evolves predominantly within the near-equilibrium domain. The nonlinear regression was performed in OriginPro using a two-stage procedure: an initial simplex search (100 iterations) to prevent divergence caused by the

strong nonlinearity of the denominator term, followed by a Levenberg–Marquardt refinement (10 iterations). This procedure yielded a stable and reproducible solution, with excellent fit statistics ($\chi^2 = 4.0 \times 10^{-5}$, $R^2 = 0.99843$).

The parameter set extracted from the exact solution includes a large composite heterogeneity factor, $B = \beta q_e \approx 31$. This single value already explains the apparent pseudo-second-order character of the curve: in the generalized Langmuir–Elovich framework, large B values make the exponential attenuation dominate the relaxation, yielding a monotonic curvature that visually mimics PSO behavior over most of the trajectory. Thus, the PSO-like shape observed by Liu et al., (2010) does not imply a true second-order mechanism—it simply reflects the strongly heterogeneous surface encoded in B.

According to Zhang's analysis, the Liu et al., (2010)system lies in an intermediate regime where neither PFO nor PSO can approximate the Langmuir kinetics. Zhang obtained a root ratio of $\theta_{e1}/\theta_{e2} = 0.648$, far from both limiting conditions (→ 0 for PFO and → 1 for PSO). Thus, under Zhang's criterion the system cannot be assigned to either simplified model. Although empirical PSO fitting appears successful, Zhang notes that this is inappropriate because the root ratio places the system outside the PSO domain.

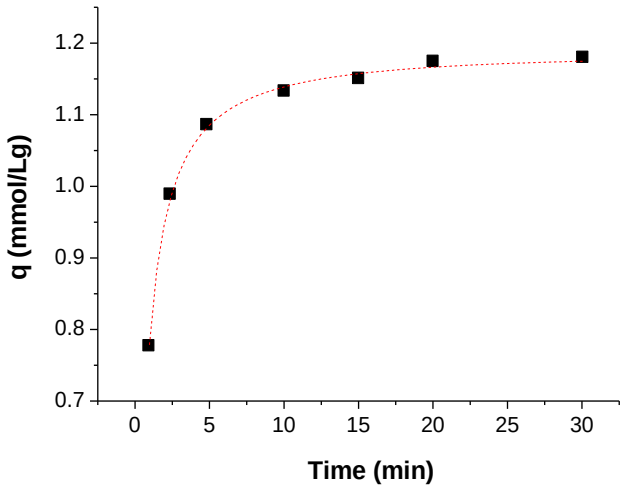

Figure 4 - Kinetic uptake of phenol on activated carbon fibers from the dataset of Liu et al (Liu et al., 2010). The black squares (■) represent experimental points digitized from the original publication using WinPlotDigitizer, and the red dashed line corresponds to the fit obtained with the exact integrated form of the generalized Langmuir–Elovich equation (Eq. 40).

When the full analytical solution is applied, however, the discrepancy is resolved. The kinetic trace reported by Liu et al., (2010) corresponds precisely to what the generalized Langmuir–Elovich model predicts for a system with $B = \beta q_e \gg 1$. Hence, while Zhang's criterion renders the model indeterminate, our criterion provides a clear diagnosis: the large value of $B \approx 31$ drives a quadratic rate decay that is effectively indistinguishable from PSO. This explains why Liu's PSO fit succeeds without contradicting Zhang's mechanistic interpretation.

Luo et al.,(2015)

Luo et al. (2015) investigated phenol adsorption on HMBP–modified montmorillonite and interpreted the kinetics using the PSO model. Zhang (Zhang, 2023), however, re-evaluated the dataset and, based on her root-ratio θ_{e1}/θ_{e2}, classified the system in the PFO domain despite its excellent PSO correlation. Because the experiment was conducted at a single initial concentration, the $\ln(k/C_{eq})$method could not be applied. To bypass this limitation, we obtained βq_e by fitting the near-equilibrium exact solution (Eq. 40). The kinetic trace lies predominantly in the near-equilibrium region $q(t)/q_e > 0.7$, allowing a clear determination of the coverage-dependent attenuation encoded in $\beta\varepsilon$.

The fit shown in Figure 5 yields the parameter set: $A = 1.59 \times 10^{-6}\, min^{-1}$, $B = \beta q_e = 3.02x10^5$ and $q_e = 0.08678\, mmol g^{-1}$, which has clear mechanistic implications. The intrinsic first-order coefficient A tends essentially to zero, while the composite heterogeneity parameter $B = \beta q_e$diverges to extremely large values. Under these conditions, the linear term $A\,\varepsilon$ becomes negligible, and the generalized rate law is governed entirely by the quadratic term $\beta A\,\varepsilon^2$. Mathematically, this corresponds exactly to the pseudo-second-order (PSO) limit of the integrated solution. When $A \to 0$and $B \to \infty$while the product ABremains finite, the general expression. $q(t) = q_e - \frac{q_e e^{-At}}{1+B(1-e^{-At})}$ reduces to $q(t) = \frac{k_2 q_e^2 t}{1+k_2 q_e t}$ (with the identification $k_2 q_e = AB$), which is the classical integrated form of the PSO model.

Thus, even though Zhang (Zhang, 2023)classified the Luo et al., (2015) dataset within the pseudo-first-order region using the root-ratio criterion, our analysis shows that the full analytical solution naturally converges to the PSO manifold for this system. The PSO-like behavior observed experimentally is therefore not an artefact of curve fitting, but the mechanistically expected outcome of operating in the strong-heterogeneity limit of the generalized Langmuir–Elovich kinetics.

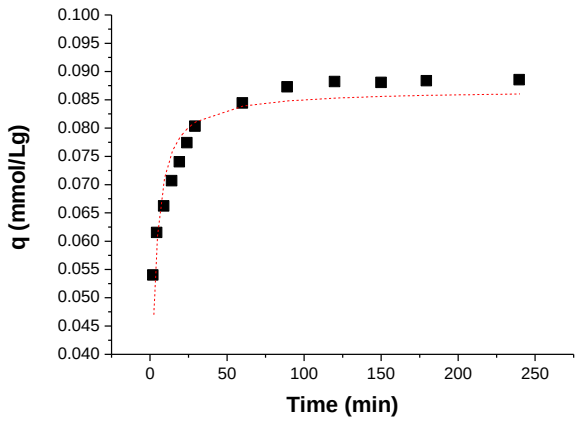

Figure 5. Kinetic uptake curve extracted from Luo et al.,(2015) for phenol adsorption onto HMBP-modified montmorillonite at 25 °C. The black squares (■) represent experimental points digitized from the original publication using WinPlotDigitizer, and the red dashed line corresponds to the fit obtained with the exact integrated form of the generalized Langmuir–Elovich equation (Eq. 40).

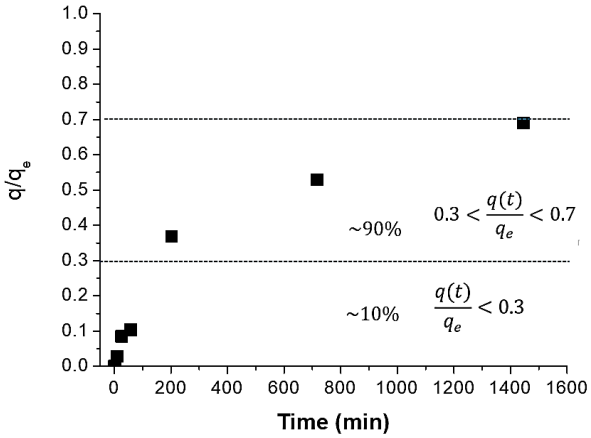

Figure 6 - Normalized coverage–time plot $q(t)/q_e$for the phenol–TCAC system at the lowest initial concentration $C_0 = 50mg/L$ reported by Khare and Kumar (2012) (■). The experimental kinetic points were digitized from Fig. 6 and Table 4 of the original publication and processed in WinPlotDigitizer. The resulting trajectory lies predominantly within the intermediate-coverage domain $0.3 < q(t)/q_e < 0.7$, with only a small fraction of points below 0.3 and none above 0.7.

Khare and Kumar (2012)

Khare and Kumar (2012) investigated the removal of phenol using Terminalia chebula–activated carbon (TCAC) and interpreted their kinetic data using the pseudo-first-order (PFO) model, based solely on the empirical correlation coefficient. When the system is examined using Zhang's solute-to-capacity criterion (Zhang, 2023), expressed as the dimensionless ratio C_0/β_A, PFO behavior is expected in the asymptotic limits $C_0/\beta_A \to 0$ or $C_0/\beta_A \to \infty$, whereas PSO behavior is associated with values close to unity. For the TCAC system, the parameters reported by Khare and Kumar (2012) place the system in an intermediate regime, far from both asymptotic limits and from the PSO condition $C_0/\beta_A \approx 1$. Accordingly, the kinetic trajectory cannot be reduced to either PFO or PSO, and the use of empirical pseudo-order models does not provide a valid mechanistic approximation of the Langmuir rate law.

Figure 6 shows the normalized coverage–time trajectory $q(t)/q_e$ reconstructed from the lowest-concentration dataset (C_0 = 50 mg L^{-1}) reported by Khare and Kumar (Khare and Kumar, 2012). The kinetic points were digitized using PlotDigitizer and subsequently processed and replotted in OriginPro 2023. As the coverage evolution lies almost entirely within the intermediate region $0.3 < q(t)/q_e < 0.7$, neither the near-equilibrium approximation nor the pure Elovich low-coverage form can be invoked for this system. It is important to note that Zhang's framework cannot capture this nuance, since the root-ratio criterion is unable to distinguish the mechanistic features characteristic of this intermediate-coverage domain.

Because the TCAC kinetic trajectory lies almost entirely within the intermediate-coverage domain $0.3 < q(t)/q_e < 0.7$, none of the asymptotic simplifications of the generalized Langmuir–Elovich rate law (i.e., the low-coverage Elovich form or the near-equilibrium expansion) can be applied. For this reason, the complete differential equation, $\frac{dq}{dt} = \alpha\, C_0\, e^{-\beta q}\,(q_e - q)$ (Eq. 13), was integrated numerically using Python (v. 3.14.2) and SciPy's adaptive Runge–Kutta solver (solve_ivp). The kinetic parameters α, β, and q_e were then obtained by nonlinear least-squares optimization (scipy.optimize.least_squares), minimizing the squared deviation between the numerical trajectory and the experimental q(t) data. This procedure allows the heterogeneity factor $\beta q_e$to be extracted directly from the curvature of the relaxation profile, without relying on pseudo-order approximations. Because only a single initial concentration is available, our $\ln(k/C_{eq})$analysis cannot be applied. Moreover, when examined through Zhang's solute-to-capacity criterion C_0/β_A, the TCAC system falls in an intermediate regime, far from both asymptotic PFO limits ($C_0/\beta_A \to 0$ or $\to \infty$) and from the PSO condition ($C_0/\beta_A \approx 1$). As a result, neither PFO nor PSO provides a valid mechanistic description for this system, reinforcing the need for the full numerical solution.

Figure 7 compares the experimental kinetic data reported by Khare and Kumar (2012) with two independent re-analyses performed in the present work: a non-linear PFO fit (blue dashed line) and the numerical integration of the GLE kinetic equation (red dashed line). While the original study interpreted the system using a linearized PFO expression, the comparison shows that even a properly fitted non-linear PFO model fails to capture the full curvature of the kinetic trajectory. In contrast,

the numerical solution of the generalized Langmuir–Elovich equation reproduces the experimental data over the entire time domain.

Notably, Khare and Kumar (2012)applied the linear PFO model and obtained $q_{cal} = 8.38\, mg\, g^{-1}$ which is substantially lower than the experimental uptake $q_{24h} = 11.35\, mg\, g^{-1}$ This discrepancy arises because the PFO model was evaluated before true equilibrium was reached, leading to an intrinsic underestimation of the adsorption capacity in the intermediate-coverage regime. In contrast, the numerical integration of the generalized Langmuir–Elovich rate law (red dashed line) yields an equilibrium capacity of $q_e \approx 10\, mg\, g^{-1}$, which is consistent with the observed kinetic trajectory and its slow relaxation toward equilibrium. The mechanistic solution accurately reproduces both the magnitude and curvature of the adsorption profile, capturing features that PFO-based models fail to describe. Furthermore, the fitted parameter βq_e provides a direct measure of energetic heterogeneity in the intermediate Langmuir regime, supplying precisely the mechanistic insight that Zhang identified as missing from empirical pseudo-order analyses.

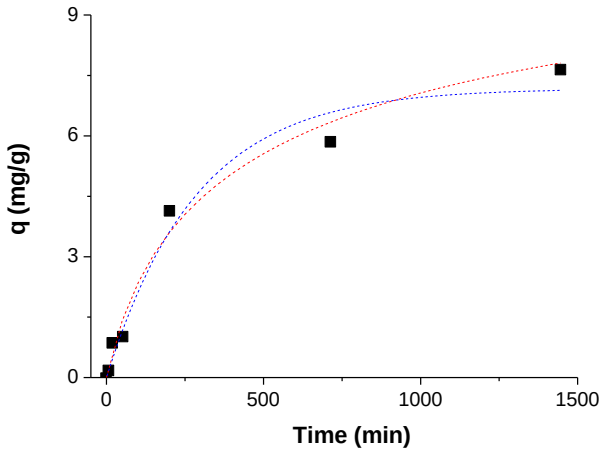

Figure 7. Kinetic data for phenol adsorption onto TCAC reported by Khare and Kumar (2012) (■), extracted by digitalization of the original plot, together with two re-analyses performed in the present work: a non-linear PFO fit (blue dashed line) obtained using OriginPro, and the numerical fit obtained by integrating the full generalized Langmuir–Elovich rate law (red line). The continuous trajectory was computed by solving the differential equation using Python (v. 3.14.2) and SciPy's adaptive Runge–Kutta integrator (solve_ivp), with parameters optimized via nonlinear least-squares fitting.

The parameters $\alpha \approx 7.0\, x\, 10^{-5} L\, mg^{-1}\, min^{-1}$ and $\beta \approx g\, mg^{-1}$ were determined through nonlinear least-squares fitting based on the numerical integration of the generalized Langmuir–Elovich rate law. Thus, the advantage of the present modeling is not merely numerical, but conceptual. While Zhang demonstrated that the phenol–TCAC kinetics cannot be classified as PFO or PSO and emphasized that no rate equation had been formulated for the intermediate regime, the generalized Langmuir–Elovich framework employed here provides precisely this missing alternative. By offering a physically grounded mechanistic description, the present analysis resolves the ambiguity highlighted by Zhang and establishes a coherent kinetic law for systems that fall outside the conventional PFO/PSO dichotomy.

Conclusion

In this work, we examined a coverage-dependent adsorption rate equation as an effective formalism for connecting Elovich, pseudo-first-order (PFO), and pseudo-second-order (PSO) behaviors. The analysis shows that the low-coverage limit recovers Elovich-like kinetics, whereas the near-equilibrium region may become effectively PFO- or PSO-like depending on the magnitude of a composite coverage parameter. An intermediate regime also emerges in which neither pseudo-order approximation is expected to be fully adequate.

The proposed approach should therefore be viewed primarily as a tool for kinetic interpretation and regime classification rather than as a microscopic theory of surface heterogeneity. Application to representative literature datasets illustrates how the formalism can help explain why different empirical models may succeed in different coverage domains and why some adsorption curves require direct numerical treatment of the full generalized rate equation.

.

References

Al-Ghouti, M.A.; Da'ana, D.A. Guidelines for the use and interpretation of adsorption isotherm models: A review. *Journal of Hazardous Materials*. 393:122383. 2020. doi:10.1016/j.jhazmat.2020.122383.

Azizian, M. Kinetic models of sorption: A theoretical analysis. *Journal of Colloid and Interface Science*. 276(1):47–52. 2004. doi:10.1016/j.jcis.2004.03.007.

Azizian, S.; Bashiri, H. Adsorption kinetics at the solid/solution interface: Statistical rate theory at initial times of adsorption and close to equilibrium. *Langmuir*. 24(20):11669–11676. 2008. doi:10.1021/la802288p.

Azizian, S.; Yahyaei, B. Adsorption of 18 crown 6 from aqueous solution on granular activated carbon: A kinetic modeling study. *Journal of Colloid and Interface Science*. 299(1):112–115. 2006. doi:10.1016/j.jcis.2006.01.058.

Ghaedi, M.; Golestani Nasab, A.; Khodadoust, S.; Rajabi, M.; Azizian, S. Application of activated carbon as adsorbents for efficient removal of methylene blue: kinetics and equilibrium study. *Journal of Industrial and Engineering Chemistry*.

20(4):2317–2324. 2014. doi:10.1016/j.jiec.2013.10.007.

Huang, Y.-T.; Shih, M.-C. Kinetic, isotherm, and thermodynamic modeling of methylene blue adsorption using natural rice husk: a sustainable approach. *Separations*. 12(8):189. 2025.

Khare, P.; Kumar, A. Removal of phenol from aqueous solution using carbonized *Terminalia chebula*-activated carbon: process parametric optimization using conventional method and

Taguchi's experimental design, adsorption kinetic, equilibrium and thermodynamic study. *Applied Water Science*. 2:317–326. 2012. doi:10.1007/s13201-012-0047-0.

Lagergren, S. About the theory of so-called adsorption of soluble substances. *Kungliga Svenska Vetenskapsakademiens Handlingar*. 24:1–39. 1898.

Liu, Q.S.; Zheng, T.; Wang, P.; Jiang, J.P.; Li, N. Adsorption isotherm, kinetic and mechanism studies of some substituted phenols on activated carbon fibers. *Chemical Engineering Journal*. 157:348–356. 2010. doi:10.1016/j.cej.2009.11.013.

Luo, Z.; Gao, M.; Yang, S.; Yang, Q. Adsorption of phenols on reduced-charge montmorillonites modified by bispyridinium dibromides: Mechanism, kinetics and thermodynamics studies. *Colloids and Surfaces A: Physicochemical and Engineering Aspects*. 482:222–230. 2015. doi:10.1016/j.colsurfa.2015.05.014.

Marczewski, A.W. Analysis of Kinetic Langmuir Model. Part I: Integrated Kinetic Langmuir Equation (IKL): A New Complete Analytical Solution of the

Langmuir Rate Equation. *Langmuir*. 39(25):8854–8867. 2010. doi:10.1021/acs.langmuir.3c00639.

Marczewski, A.W.; Deryło-Marczewska, A.; Słota, A. Adsorption and desorption kinetics of benzene derivatives on mesoporous carbons. *Adsorption*. 19(2–4):391–406. 2013. doi:10.1007/s10450-012-9462-7.

Marczewski, A.W.; Seczkowska, M.; Deryło-Marczewska, A.; Blachnio, M. Adsorption equilibrium and kinetics of selected phenoxyacid pesticides on activated carbon: effect of temperature. *Environmental Science and Pollution Research*. 25(11):10846–10860. 2018. doi:10.1007/s11356-017-0682-6.

Salvestrini, S. Analysis of the Langmuir rate equation in its differential and integrated form for adsorption processes and a comparison with the pseudo first and pseudo second order models. *Reaction Kinetics,*

Mechanisms and Catalysis. 123(2):455–472. 2018. doi:10.1007/s11144-017-1295-7.

Zhang, J. Physical insights into kinetic models of adsorption. *Separation and Purification Technology*. 314:123585. 2023. doi:10.1016/j.seppur.2023.123585.

Zohra, F.-T.; Ahmed, S.; Alam, M.Z.; Nurnabi, M.; Rahman, N. Bio-waste to environmental purifier: Application of potato peel for acid red 73 adsorption from leather dyeing effluent. *Water Resources and Industry*. 33:100281. 2025. doi:10.1016/j.wri.2025.100281.